Research Article | Vol. 13, No. 9 / 1 Sep 2022 / Biomedical Optics Express 4706

Biomedical Optics EXPRESS

In vivo tracking of individual stem cells labeled with nanowire lasers using multimodality imaging

XUZHOU LI,[1,2,6] WEI ZHANG,[1,6] YANXIU LI,[3,4,6] XIAOQIN WU,[5] MINGYANG WANG,[1] XIAOTIAN TAN,[1] YANNIS M. PAULUS,[1,4,7] XUDONG FAN,[1,8] AND XUEDING WANG[1,*]

[1]*Department of Biomedical Engineering, University of Michigan, Ann Arbor, MI 48109, USA*
[2]*Department of Mechanical Engineering, University of Michigan, Ann Arbor, MI 48109, USA*
[3]*Eye Center of Xiangya Hospital, Hunan Key Laboratory of Ophthalmology, Central South University, Changsha, Hunan 410008, China*
[4]*Department of Ophthalmology and Visual Sciences, University of Michigan, Ann Arbor, MI, 48105, USA*
[5]*Key Laboratory of Optoelectronic Technology & Systems (Ministry of Education), Chongqing University, Chongqing 400044, China*
[6]*These authors contribute equally to this work*
[7]*ypaulus@med.umich.edu*
[8]*xsfan@umich.edu*
[*]*xdwang@umich.edu*

Abstract: Emerging cell-based regenerative medicine and stem cell therapies have drawn wide attention in medical research and clinical practice to treat tissue damage and numerous incurable diseases. *In vivo* observation of the distribution, migration, and development of the transplanted cells is important for both understanding the mechanism and evaluating the treatment efficacy and safety. However, tracking the 3D migration trajectories for individual therapeutic cells in clinically relevant pathological environments remains technically challenging. Using a laser photocoagulation model in living rabbit eyes, this study demonstrates a multimodality imaging technology integrating optical coherence tomography (OCT), fluorescence microscopy (FM), and lasing emission for *in vivo* longitudinal tracking of the 3D migration trajectories of individual human retinal pigment epithelium cells (ARPE-19) labeled with CdS nanowires. With unique lasing spectra generated from the subtle microcavity differences, the surface-modified nanowires perform as distinct spectral identifiers for labeling individual ARPE-19 cells. Meanwhile, with strong optical scattering and natural fluorescence emission, CdS nanowires also served as OCT and FM contrast agents to indicate the spatial locations of the transplanted ARPE-19 cells. A longitudinal study of tracking individual ARPE-19 cells in rabbit eyes over a duration of 28 days was accomplished. This method could potentially promote an understanding of the pharmacodynamics and pharmacokinetics of implanted cells in the development of cell-based therapies.

1. Introduction

Emerging cell-based therapies such as regenerative medicine therapies (RMTs) and stem cell therapies have attracted significant interest as potential treatment options for severe tissue damages and numerous currently incurable diseases [1–4]. In many cell-based therapies, transplanted cells are administered close to the damaged tissue to migrate towards and stay within the damaged tissue, and then replicate and differentiate into multiple cell types to restore the structure and function of the targeted regions [2,5,6]. For instance, several clinical trials have been conducted for administering retinal pigment epithelium (RPE) cells via subretinal injections for RPE degeneration restoration in the retina in geographic atrophy of macular degeneration

#454558 https://doi.org/10.1364/BOE.454558
Journal © 2022 Received 8 Apr 2022; revised 2 Jun 2022; accepted 17 Jul 2022; published 11 Aug 2022

Biomedical Optics EXPRESS

[6–9]. After being introduced into the subretinal space, the transplanted RPE cells can create a functional RPE layer to replace the damaged original RPE as a part of the photoreceptor restoration process. Despite the great promise of this cell-based therapeutic method, the lack of comprehensive understanding of the migration, replication, and fate of the transplanted cells remains a major obstacle in clinical application. As the traditional method to evaluate therapeutic efficacy and safety, histological analysis can only provide limited information due to its invasive and destructive nature [10,11]. Therefore, novel technologies that can directly and precisely monitor the 3D distribution and migration of implanted cells *in vivo* and longitudinally are highly desired.

Many imaging techniques, such as fluorescence microscopy (FM) and optical coherence tomography (OCT), have been applied in labeling and tracking transplanted cells [12–15], especially in visualizing the stem cells on the retina [16]. Fluorescence labeling is another widely used technique in differentiating various targets and tracking cell migration [12,13,17]. Researchers has achieved precise locating GFP labeled cells with scanning laser ophthalmoscopy (SLO) and OCT multimodality imaging system [18], which brings significant impact in cell therapy in ophthalmology.

In addition, multi-spectral fluorescence labels were exploited to provide distinguishable information to track different cell groups *in vivo* with various light emission spectra from different colors of fluorophores [13]. However, due to the nature of broad emission spectra of fluorophores, the total available different labels involved in multi-spectral fluorescence imaging are limited. In addition, as a result of low efficiency and photobleaching, fluorescence dyes usually cannot enable a high signal-to-noise ratio for single cell tracking or support longitudinal studies over extensive time periods which are necessary for cell-based regenerative therapies. More importantly, for *in vivo* applications, the conventional FM images can only provide 2D information but not 3D information, which is crucial for studying the interaction of cells with the surrounding tissue. Even though three photon microscopy and confocal microscopy could provide decent 2D resolution and some 3D information [19,20], they are suffering from low signal intensity or limited imaging depth in tissue. OCT is a clinically available 3D imaging technology with ultra-high resolution and excellent imaging depth [21,22] and has shown great potential for *in vivo* cell tracking. Contrast agents such as gold nanoparticles [23,24], polymer, and metal oxide nanoparticles [25,26] with strong scattering properties have been applied to label target cells to improve imaging visibility. However, since the optical properties of most contrast agents are homogenous, the current OCT-based technique is only capable of monitoring the overall distributions of labeled cells. 3D longitudinal tracking of individual cells *in vivo* still remains a technical challenge.

Microcavity laser emission-based imaging is an emerging technology in biomedical research. Owing to the small size, high emission intensities, narrow linewidth, and abundant spectral information, the microcavity lasers have shown great potential in intracellular labeling [27–29] and microenvironmental sensing [30–34]. The hundred-fold narrower emission linewidth and higher signal-to-noise ratio of intracellular microcavity lasers have demonstrated great advantages over the traditional fluorescence labeling. The unique lasing spectra with multiple peaks with nanometer-level linewidth determined by the varying cavity structure could serve as "identifiers" for differentiating individual cells. Encoded with a "serial number" formed by the lasing peak positions of the microcavity lasers, a large number of cells can be individually tracked at the same time. However, similar to FM, the *in vivo* tracking based on lasing emission provides only 2D images and the critical 3D location information cannot be captured.

In this study, we demonstrated a multimodality imaging technology combining OCT, FM, and lasing emission labeling to longitudinally track the *in vivo* 3D migration trajectories of individual retinal pigment epithelium (ARPE-19) cells transplanted into the subretinal space. The rabbit model involved in this study was laser-induced retinal pigment epithelium (RPE)

Biomedical Optics EXPRESS

photocoagulation injury in the retina. The surface-modified CdS nanowire lasers, with the distinct lasing spectra generated from the subtle microcavity differences, were utilized as unique identifiers to label the transplanted ARPE-19 cells. Meanwhile, with strong optical scattering and fluorescence emission, CdS nanowires also served as OCT and FM contrast agents to indicate the spatial locations of the transplanted ARPE-19 cells. Specifically, OCT could provide the precise spatial coordinates while FM could help cross validate to avoid noise interference. In this work, this dual-modality contrast along with the differentiable identifiers provided by the lasing spectra of CdS nanowires built the fundamental for *in vivo* single cell tracking. After the ARPE-19 cells labeled with CdS nanowires were implanted, FM could provide the overall 2D cell distribution pattern, whereas the nanowires internalized by the cells were pumped to provide unique lasing emission spectra for differentiating individual cells. At the same time, OCT en-face imaging could provide both 3D retinal structure and spatial locations of the cells, which were cross-validated with the FM images. Thus, by integrating the capabilities of FM, OCT, and lasing emission labeling, this multimodality imaging method achieved longitudinal 3D tracking of individual cells in the subretinal space *in vivo* for the first time.

2. Material and methods

2.1. Experiment setup

An OCT, FM, and lasing emission spectra multimodality imaging system was utilized for *in vivo* single cell tracking in this study. As shown in Fig. 1(a), a spectral-domain OCT (SD-OCT) was integrated with the fluorescence detection photodiode and lasing measurement spectrometer. A broadly tunable pulsed diode-pumped solid-state laser working at 485 nm was coaxially combined with the OCT light to provide fluorescence and lasing excitation and ensure the co-registration between different imaging modalities. The OCT reflection, fluorescence, and lasing emission were collected and measured from the backward optical path of the telescope configuration. More details of the multimodality imaging system are included in Supplementary information. The ARPE-19 cells were labeled with CdS nanowires and introduced into the subretinal space of the rabbits with laser-induced injuries in the retina Fig. 1(b). The OCT and FM images were employed for cell spatial location extraction, whereas the lasing emission spectra of the nanowires served as identifiers.

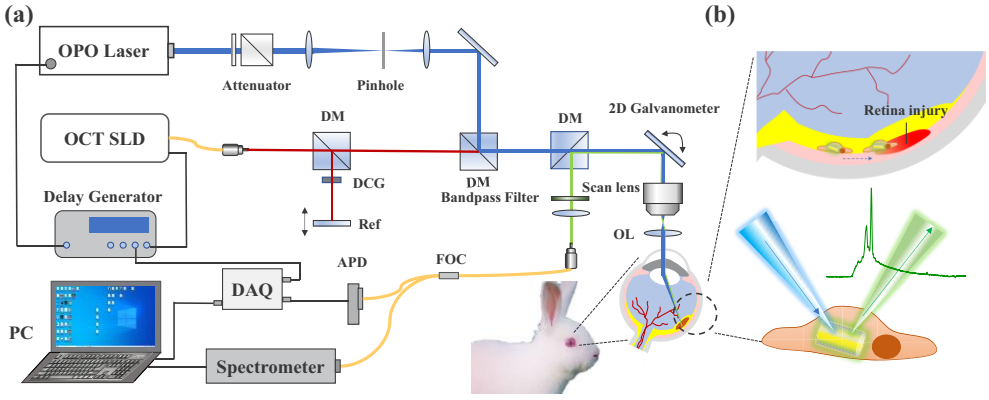

Fig. 1. (a) Schematic of the optical coherence tomography (OCT), fluorescence microscopy, (FM), and laser emission multimodality imaging system. APD: Avalanche photodiode; DAQ: Data acquisition card; DCG: Dispersion-compensation glass; FOC: Fiber optic coupler; SLD: superluminescent diode; DM: dichroic mirror; OL: ophthalmic lens; OPO: optical parametric oscillator. (b) Illustration of CdS nanowire labeled ARPE-19 cells migrating in the subretinal layer and generating lasing emission for tracking identification.

Biomedical Optics EXPRESS

2.2. ARPE-19 cell preparation

Human RPE cell line ARPE-19 is a spontaneously immortalized cell line of human retinal pigment epithelium without melanin pigment, which is widely used to study retinal cell biology, pathological conditions, and pharmacology. In addition, as a good cell line for in vitro studies of retinal pigment epithelium physiology, ARPE-19 has structural and functional properties characteristic of RPE cells in vivo and suggest that this cell line will be valuable [35]. The ARPE-19 cell line was originally acquired from a commercial vendor (ATCC, Manassas, VA). ARPE-19 cell culture media consisted of DMEM F-12 medium with 1% penicillin/streptomycin and 10% fetal bovine serum (FBS). The cells were cultured in a humidified incubator with 5% CO2 at 37 °C. All supplies were purchased from Thermo Fisher, Waltham, MA.

2.3. Preparation of animal model and CdS nanowires

In order to simulate an authentic, clinically-relevant pathological environment for cell therapy, laser-induced photocoagulation injuries of the retina and RPE were created in rabbit eyes (see details in the Supplementary information). As shown in Fig. 2(a), two arrays of laser-induced injury spots with 1-mm spacing were highlighted by arrows. The CdS nanowire lasers served as both OCT and FM contrast agents and unique identifiers (more details regarding the nanowire fabrication are described in the Supplementary information). To achieve successful cell labeling, the CdS nanowires need to be internalized into the cells. Considering the relatively large size of nanowires (3-7 μm in length and 200 nm in diameter) relative to the ARPE-19 cells (~30 μm), biocompatible surface modification of CdS nanowires is necessary. A multilayer collagen coating of CdS nanowire was achieved by a layer-by-layer (LBL) assembly method to promote internalization [36,37], as shown in Fig. 2(b) (see Supplementary information for more details). To confirm the improvement in cell internalization, the ARPE-19 cells were cultured together with surface-modified nanowires and monitored by a confocal fluorescence microscope Fig. 2(c). Here, the cell cytoskeleton and nuclei were stained blue and red, respectively, whereas the CdS could be visualized by its green fluorescence emission. From the top and right cross-sectional insets in Fig. 2(c), complete internalization of nanowires within the cell body was confirmed. As a control experiment, ARPE-19 cells cultured with bare CdS nanowires showed few nanowire internalizations (see the confocal fluorescence microscopy image in Figure S1).

Due to its high refractive index (~2.67) compared to the surrounding medium (~1.33), a CdS nanowire can be regarded as a Fabry-Perot (F-P) cavity with a CdS serving as both waveguide and gain medium [38,39]. At a low excitation energy density below the lasing threshold (1 μJ/mm^2), only ordinary green fluorescence emission was observed as the blue curve shown in Fig. 2(d). When excited at a relatively high pump energy density (5 μJ/mm^2) which was above the lasing threshold, the lasing emission was observed with multiple peaks (Fig. 2(d), red curve). The insets in Fig. 2(d) were the lasing output vs. pump energy density curve that shows a lasing energy threshold around 4 μJ/mm^2. During the CdS nanowire manufacturing and preparation, the length of nanowires was randomly distributed. Thus, the CdS nanowires had various cavity lengths and, as a result, numerous unique lasing emission spectra, facilitating labeling and identification of a large number of single cells. On the other hand, also due to its high RI and elongated shape, the CdS nanowire had strong optical scattering that significantly enhanced the OCT signal.

As shown in the OCT image in Fig. 2(e), a CdS nanowire labeled ARPE-19 cell was indicated with the yellow arrow. By analyzing the A-scan signal profile along the yellow dashed line (Fig. 2(e), right inset), the CdS nanowire was noted to provide 15 dB OCT contrast against the surrounding retina tissue *in vivo*. The capabilities of CdS nanowires to generate fluorescence emission, lasing emission, and OCT contrast form the foundation for single cell tracking *in vivo*. More detailed experiment methods were included in the supplementary document.

Biomedical Optics EXPRESS

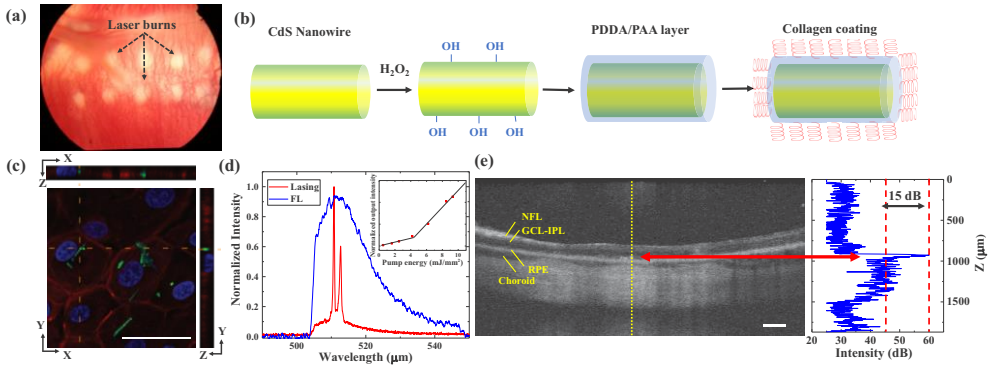

Fig. 2. (a) The color fundus image of an experimental rabbit. The two arrays of laser photocoagulation burn injuries are marked. (b) The schematic of the PDDA/PAA/collagen biocompatible coating process to promote cell internalization of CdS nanowire lasers. (c) A confocal fluorescence image of the surface-modified nanowires internalized by the ARPE-19 cells. The nanowires are labeled in green, and the cell nuclei and skeleton are labeled with blue and red, respectively. The X-Z and Y-Z cross-sectional images along the dashed lines are on the top and right. Scale bar: 50 μm. (d) A comparison of lasing emission spectra and fluorescence emission spectra. The broad blue curve (FL) is the CdS fluorescence emission spectrum, while the red curve with multiple peaks is the CdS nanowire lasing emission spectrum. The inset in the upper right is the threshold curve of CdS nanowire lasers. (e) OCT B-scan image from the experimental retina region after the injected fluid was fully resolved. The nanowire labeled ARPE-19 cells are highlighted with the red arrow and have higher contrast against the surrounding layers. The right inset is a blue signal intensity curve along the yellow dashed line indicated on the left, which demonstrates that the CdS nanowires can provide a contrast enhancement at a level of 15 dB. NFL: nerve fiber layer; GCL: ganglion cell layer; IPL: inner plexiform layer; RPE: retinal pigment epithelium layer; Scale bar: 200 μm.

3. Results

3.1. *In vivo* subretinal single cell tracking

First, the laser-induced injuries were created in the retina of experimental rabbits to generate a clinically relevant therapy microenvironment. Subsequently, after being cultured with surface modified CdS nanowires for 24 hours, the ARPE-19 cells were collected and resuspended in the cell-enriched solution. 20 μL of the cell-enriched solution was injected into the subretinal space through a subretinal injection operation (see details in the Supplementary information). Localized subretinal fluid including in the region of laser-induced injuries was observed (D1 in Fig. 3(a)). The imaging experiment for *in vivo* single cell tracking started after the fluid was fully resolved at D4 and was repeated at different time points over a period of 28 days. At each observation time, color fundus images, fluorescence microscopy, OCT en-face imaging, and lasing emission spectra were collected for retinal structure monitoring and single cell tracking. Figure 3(a) shows the color fundus images of an experiment rabbit through the period of 28 days to depict the retinal anatomy and appearance. A series of fluorescence microscopy images collected during each observation time are presented in Fig. 3(b). The black circles and blue circles in Figs. 3(a) and (b) indicate the laser-induced injury spots on the retina. As time went on after injection, an increasing number of nanowire labeled cells clustered around the injury spots which is consistent with the biological function of ARPE-19 cells. The FM played an important role in the following aspects. First, FM images depicted the overall 2D distribution of the nanowire labeled ARPE-19 cells. This information was cross-validated with the spatial locations of the cells collected from

Biomedical Optics EXPRESS

the 3D OCT scanning. In our post data processing, the precise spatial distributions of the cells were extracted from OCT en-face images by thresholding, which could be influenced by some strong scattering noise and defects in the animal tissue. The 2D cell distribution information provided by FM could filter out these noises and defects. Second, since it took 1-2 seconds to finish a lasing emission spectra collection, it would be time-consuming and impractical to scan over all the pixels. FM images after thresholding (e.g., Fig. 4(a)) along with a contour and center extraction algorithm were able to locate the nanowires within the field of view quickly such that the pump light could be delivered directly to the nanowires and their laser emission spectra could be collected subsequently.

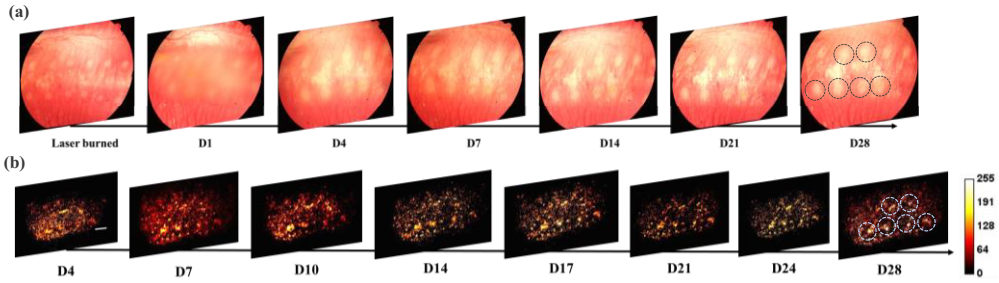

Fig. 3. (a) A series of color fundus images of the experimental retina region with laser-induced injuries. The images were acquired at different time points over a duration of 28 days. CdS nanowire labeled ARPE-19 cells were injected on Day 1 and were periodically observed starting from Day 4 after the injected fluid was fully resorbed. (b) A series of FM images collected from the same experimental retinal region as in (a) at different time points after the retina region was clear to observe (from Day 4). Scale bar: 200 μm. The black circles and blue circles in (a) and (b), respectively, highlight the locations of laser-induced injury spots.

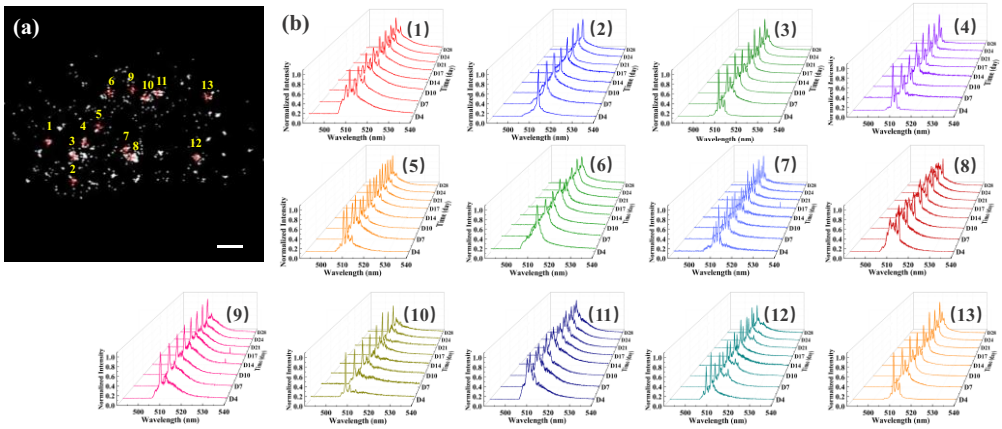

Fig. 4. (a) The instantaneous 2D locations of CdS nanowire labeled ARPE-19 cells extracted from the FM image on D4. In total, 13 cells were tracked in this result. (b) Normalized lasing spectra from the 13 identified ARPE-19 cells acquired at different time points during the period of 28 days. Each cell identity was presented by a unique lasing spectral waveform which was stable over the entire observation period.

A total of 13 cells were tracked through the experiment for Fig. 3, and their instantaneous 2D locations on D4 were marked in the thresholded FM image Fig. 4(a) as an example. The identities

Biomedical Optics EXPRESS

of the 13 tracked ARPE-19 cells were verified by the lasing emission spectra of the carried nanowires. The lasing peak wavelengths are extracted and recorded as a sequence of "barcode" for cell identity. Therefore, by comparing the barcodes of peak wavelengths as a sequence of numbers from the acquired lasing spectra at various time frames, we can verify whether the cell is the same one or not. Figure 4(b) presents the normalized lasing emission spectra acquired from the same 13 ARPE-cells as in Fig. 4(a) over time. The waveforms of lasing emission spectra from these ARPE-19 cells remained stable and distinguishable throughout the experiments over a period of 28 days.

Measuring the lasing emission spectra of CdS labeled ARPE-19 cells enabled the identification of individual cells, while the relative 3D locations of the ARPE-19 cells within the retina were acquired by OCT volume scanning. Facilitated by the strong optical scattering of CdS nanowires, the distributions of cells in an OCT image could be extracted via signal thresholding. Figure 5(a) shows a series of OCT maximum intensity projection (MIP) images in the XY plane of the same field of view. The overall retina structure was rendered in grayscale whereas the thresholded signals were labeled in yellow. The laser-induced retinal injury areas were highlighted by the red circles. Figure 5(b) demonstrates the side view of the OCT 3D rendering; the distribution of extracted labeled cells is mainly in the subretinal space, which is consistent with the original injection location. Extracting the locations of individual cells by solely thresholding OCT signals could lead to artifacts caused by the strong scattering noise and defects in the tissue. By leveraging the FM and OCT dual contrast of CdS nanowires, the FM images acquired from the same region of interest worked as cross-validation. By comparing the FM images and OCT XY plane projection, only the extracted signals which appeared in both FM and OCT images were considered as valid cells. With the overall distribution pattern provided by FM Fig. 5(c), the tracked cells in Fig. 4(a) were easily extracted in the OCT volume rendering. The top view and side view of the spatial locations of tracked cells after cross-validation with FM images are highlighted in Figs. 5(d) and (e). The red circles in Fig. 5(d) are corresponding to the laser-induced regions in Fig. 5(a) and (b).

Figure 6(a) provides a cross-sectional B-scan image from OCT scanning to demonstrate the relative positions of nanowire labeled cells and the retina structure. This B-scan image also confirmed that more ARPE-19 cells were clustered near the laser-induced injury spots. As for the spatial location extraction, the Z-axis coordinates of the cells were measured as the distance from the cell to the RPE layer of the retina. With the identity of ARPE-19 verified and 3D location precisely measured, the 3D cell migration trajectories were acquired and shown in Fig. 6(b).

To examine the repeatability of the presented imaging technology, the same study was repeated on two additional rabbits, as shown in Figures S2-S5. In addition, to confirm that the nanowire lasers tracked *in vivo* were indeed carried by the ARPE-19 cells, a control experiment was conducted by injecting nanowire solution into the subretinal space. The laser-induced injury spots were highlighted by the black circles in Fig. 7(a), and also in the FM images in Fig. 7(b) and the OCT MIP image in Figs. 7(c). In the OCT MIP and B-scan images in Figs. 7(c) and (d), the extracted nanowires were labeled with yellow. By looking at the OCT MIP image in Fig. 7(c) in combination with the FM images in Fig. 7(b), we can see that the nanowires were not clustered around the injury spots, and no significant migration of the CdS nanowires was observed during this control experiment.

After the *in vivo* experiments were finished, hematoxylin and eosin (H&E) stain histology analysis was conducted to validate the results from multimodality imaging. The H&E histological analysis of a cross-sectional slice including an area of laser-induced retinal photocoagulation injury was shown in Figs. 8(a). Meanwhile, the fluorescence microscopy image of the same region was collected under blue excitation light. The bright green dots in Fig. 8(b) were the CdS nanowires. The fluorescence microscopy image overlapped on the histology result is presented in

Biomedical Optics EXPRESS

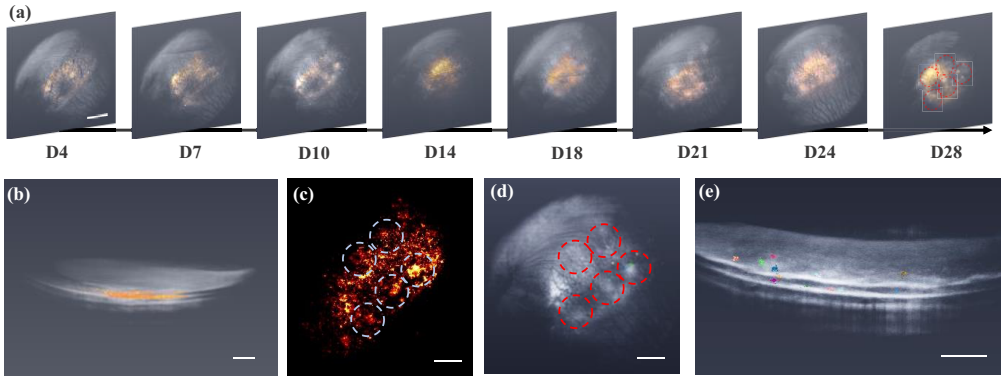

Fig. 5. (a) A series of OCT X-Y plane projection images of the same region as in Fig. 3 over the period of 28 days. The overall retinal structure is rendered in grayscale and nanowire labeled ARPE-19 cells after thresholding are highlighted in yellow. (b) The side view of the 3D rendering of D21 to show that the extracted cells are mostly distributed in the subretinal space. Scale bar: 800 µm. (c) The corresponding FM image of the same region. The distribution pattern of the fluorescence signal was used to cross-validate the extracted OCT pattern in (a), which confirmed the existence of CdS nanowire lasers and excluded noise. Scale bar: 800 µm. (d) The labeled cells corresponded to Fig. 4(a) were highlighted with various colors in the OCT 3D volume rendering. The exact spatial coordinates were extracted from OCT. Scale bar: 800 µm. The gray and red circles in (a), (c), and (d), respectively, highlighted the corresponding laser-induced retina injury spots. (e) A side view of the 3D rendering of the same cells in (c). Scale bar: 500 µm.

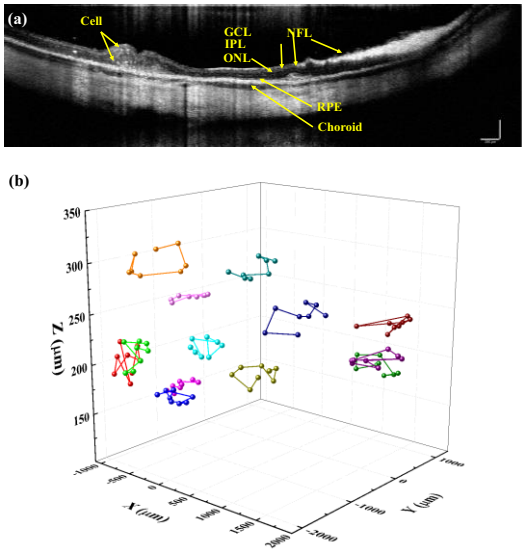

Fig. 6. (a) An OCT cross-sectional B-scan of the experimental retina region. The locations of two tracked ARPE-19 cells labeled with nanowire lasers were indicated with arrows. The retinal layer structures were presented as well. Scale bar: 250 µm. (b) The *in vivo* 3D ARPE-19 cell migration trajectories (13 cells in total) extracted from OCT volume scans acquired at different time points over the 28-day observation period. The z-axis coordinates of the tracked cells were measured by the distance between the cells and the RPE layer of the retina.

Biomedical Optics EXPRESS

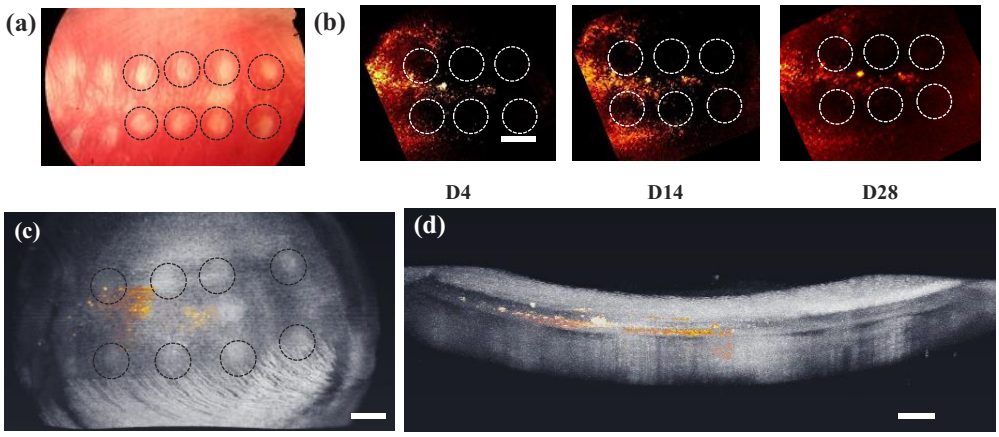

Fig. 7. (a) A color fundus image of the experimental retina. The laser photocoagulation injuries were highlighted with black dashed circles. (b) A series of FM images of the subretinal region acquired at several observation time points after injection of CdS nanowire solution (not internalized by the ARPE-19 cells). The laser-induced injury spots are highlighted by the white circles. Scale bar: 800 µm. (c) The X-Y plane projection of the OCT 3D rendering. The overall retina structure is rendered in gray and the extracted nanowires are labeled in yellow. The laser burn injuries are highlighted with black circles. (d) The XZ side view of the 3D OCT rendering as in (c). Scale bar: 250 µm.

Fig. 8(c), which verified the clustering of the nanowire labeled ARPE-19 cells in the laser-induced injury region.

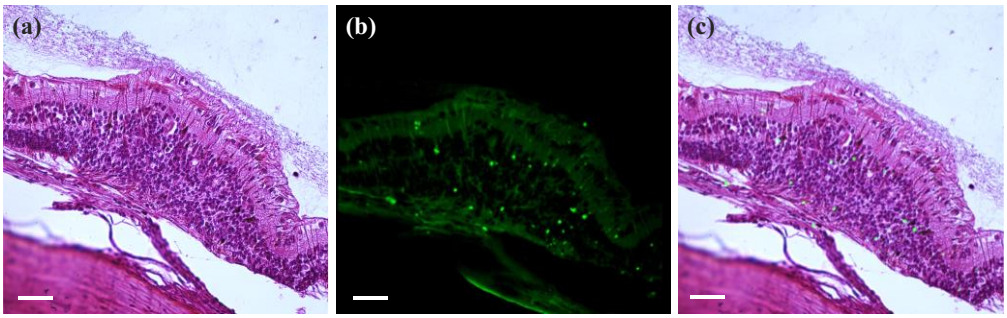

Fig. 8. (a) H&E stain histology photo of a retina slice containing a laser-induced injury region. Scale bar: 50 µm. (b) The fluorescence microscopy image of the same region as in (a). The bright green spots are CdS nanowires. Scale bar: 50 µm. (c) The fluorescence microscopy image overlapped on the H&E stain photo, indicating the CdS nanowires clustering in the laser-induced injury region.

4. Conclusion and discussion

In this study, we demonstrated 3D longitudinal tracking of individual ARPE-19 cells *in vivo* with a multimodality imaging system integrating OCT, FM, and lasing emission. The surface-modified CdS nanowires were internalized by ARPE-19 cells and provided both OCT and FM contrast enhancement for precise spatial location extraction and unique lasing emission spectra for cell identification. The nanowire labeled ARPE-19 cells were injected into the subretinal space where laser-induced injuries were created to generate a pathological environment for cell therapy.

Biomedical Optics EXPRESS

By integrating 2D and 3D spatial information and the spectral identifying information from each imaging modality, over 10 transplanted cells were monitored individually and tracked longitudinally for 28 days. The overall cell distribution and 3D migration trajectories of individual cells carrying the CdS nanowires were acquired successfully from the FM images and OCT images. The imaging results validated the clustering of the therapeutic ARPE-19 cells within the laser-induced injury areas in the retina as a result of cell migration after subretinal injection. This imaging finding was later confirmed by histology analysis of the retinal tissue slices.

Compared to our previous study [15], we pushed this single cell tracking technology by several important steps towards real-world clinical applications. First, in this study, the ARPE-19 cells were tracked in the damaged retina region, which is a clinically meaningful situation to further prove the feasibility of this technology. Second, the longitudinal study was extended from 3 days to 28 days to capture more meaningful information. Third, by improving the resolution of our spectrometer from 0.3 nm to 0.07 nm, more lasing peaks could be identified clearly in this study. Thus, more "identifier digits" could help improve the number of distinct labels. Compared to three cells tracked last time, in this study, 10 + cells were tracked in 3 rabbits to confirm the improvement in cell tracking. Fourth, the previous study used macrophages, which are very large cells that are adept at phagocytosing material, whereas this study utilized smaller ARPE-19 cells which are being used for regenerative medicine therapies and clinical utilization of cell imaging technologies. It is important to highlight the differences between CdS nanowire and semiconductor quantum dots. Semiconductor quantum dots are also light-emitting particles that are widely applied in labeling biomedical targets. Compared to nanowires, quantum dots are much smaller in size (2-10 nm) and, hence, cannot form lasing resonant cavities. Therefore, the emission (i.e., fluorescence) linewidth of quantum dots is much wider than that of CdS nanowires. In addition, fluorescence from a quantum dot has only one emission peak, whose spectral location depends on their size and material, while laser emission from nanowires has multiple peaks coming from the numerous lasing modes. This means that quantum dots are not able to provide differentiable identifiers for a large number of individual cells. On the other hand, due to the small size of quantum dots, the optical scattering property is extremely weak for providing OCT contrast so that 3D information of the labeled cells is also not accessible.

There are several aspects of this technology which could be further improved. First, Cd is considered as toxic for human so that this CdS nanowire-based technology could not be directly translated to clinical study. However, with the technology concept been proved, in the future, non-toxic material will be studied as a practical contrast agent for real clinical translation. Second, the repetition rate of our excitation laser was only 1 kHz. As a result, it took minutes to finish the FM scan, which is time-consuming and introduces unnecessary noise and artifacts. The system could be upgraded by using a laser with a high repetition rate to improve the imaging speed significantly. Third, in our current study, the unique lasing spectrum of CdS nanowire came from the random distribution of the nanowire structures. In order to obtain more unique labels and better control of the lasing emission spectral distribution, improvement in microfabrication and design of microcavity lasers are necessary. Last, even though the spectrometer in this study has been upgraded to have better spectral resolution compared to our previous study [15], the thermal noise during the spectrum collection impaired the overall signal-to-noise ratio. To address this problem, a cooled spectrometer may be used for future studies.

Pharmacodynamics (PD) and pharmacokinetics (PK) of transplanted cells are one of the major concerns in state-of-the-art cell-based regenerative medicine and translational applications. The capability to precisely and non-invasively track single cell migration *in vivo* can contribute to the understanding of the PD and PK of cell-based therapies for a comprehensive evaluation of both safety and efficacy. Our technology, by leveraging the advantages of OCT, FM, and lasing emission from surface-modified CdS nanowire lasers, showed the feasibility for 3D tracking the migrations of transplanted progenitor cells accurately and longitudinally in the large-animal

Biomedical Optics EXPRESS

subretinal space *in vivo*. The single-cell tracking capability presented in this work could serve as a platform technology to shed new light on understanding the PD and PK of cell-based therapies in ophthalmology and other medical fields. In addition, our technology also holds potential in supporting basic research on biological mechanisms *in vivo* and *in vitro*, such as longitudinal tracking of cell migrations and interactions in organoids and artificial tissues.

Funding. NSF (ECCS-1607250); NIH (K08EY027458, R01EY029489).

Disclosures. The authors declare no conflicts of interest.

Data availability. Data underlying the results presented in this paper are not publicly available at this time but may be obtained from the authors upon reasonable request.

Supplemental document. See Supplement 1 for supporting content.

References

1. V. F. Segers and R. T. Lee, "Stem-cell therapy for cardiac disease," Nature **451**(7181), 937–942 (2008).
2. T. G. Koch, L. C. Berg, and D. H. Betts, "Current and future regenerative medicine—principles, concepts, and therapeutic use of stem cell therapy and tissue engineering in equine medicine," Can. Vet. J. **50**(2), 155 (2009).
3. A. M. Bailey, M. Mendicino, and P. Au, "An FDA perspective on preclinical development of cell-based regenerative medicine products," Nat. Biotechnol. **32**(8), 721–723 (2014).
4. T. Liu Z., M. Zhao J, R. Chai, and J. Kang, "Looking into the Future: Toward Advanced 3D Biomaterials for Stem-Cell-Based Regenerative Medicine," Adv. Mater. **30**(17), 1705388 (2018).
5. V. Chichagova, D. Hallam, J. Collin, D. Zerti, B. Dorgau, M. Felemban, M. Lako, and D. H. Steel, "Cellular regeneration strategies for macular degeneration: past, present and future," Eye **32**(5), 946–971 (2018).
6. Q. Y. Li, T. Zou, Y. Gong, S. Y. Chen, Y. X. Zeng, L. X. Gao, C. H. Weng, H. W. Xu, and Z. Q. Yin, "Functional assessment of cryopreserved clinical grade hESC-RPE cells as a qualified cell source for stem cell therapy of retinal degenerative diseases," Exp. Eye Res. **202**, 108305 (2021).
7. Z. Ablonczy, M. Dahrouj, P.H. Tang, Y. Liu, K. Sambamurti, A.D., Marmorstein, and C.E. Crosson, "Human retinal pigment epithelium cells as functional models for the RPE in vivo. Investig," Ophthalmol. Vis. Sci. 52(12), 8614–8620 (2011).
8. L. Hellinen, L. Pirskanen, U. Tengvall-Unadike, A. Urtti, and M. Reinisalo, "Retinal pigment epithelial cell line with fast differentiation and improved barrier properties," Pharmaceutics **11**(8), 412 (2019).
9. M. Zarbin, I. Sugino, and E. Townes-Anderson, "Concise review: update on retinal pigment epithelium transplantation for age-related macular degeneration," Stem Cells Transl. Med. **8**(5), 466–477 (2019).
10. A. M. Timmers, H. Zhang, A. Squitieri, and C. Gonzalez-Pola, "Subretinal injections in rodent eyes: effects on electrophysiology and histology of rat retina," Mol. Vis. **7**, 131–137 (2001).
11. M. Trieschmann, F. J. G. M. Van Kuijk, R. Alexander, P. Hermans, P. Luthert, A. C. Bird, and D. Pauleikhoff, "Macular pigment in the human retina: histological evaluation of localization and distribution," Eye **22**(1), 132–137 (2008).
12. A. F. L. Schneider and C. P. R. Hackenberger, "Fluorescent labelling in living cells," Curr. Opin. Biotechnol. **48**, 61–68 (2017).
13. C. T. Kuo, H. S. Peng, Y. Rong, J. Yu, W. Sun, B. Fujimoto, and D. T. Chiu, "Optically encoded semiconducting polymer dots with single-wavelength excitation for barcoding and tracking of single cells," Anal. Chem. **89**(11), 6232–6238 (2017).
14. E. D. SoRelle, D. W. Yecies, O. Liba, F. C. Bennett, C. M. Graef, R. Dutta, S. Mitra, L. M. Joubert, S. Cheshier, G. A. Grant, and A. de la Zerda, "Spatiotemporal tracking of brain-tumor-associated myeloid cells in vivo through optical coherence tomography with plasmonic labeling and speckle modulation," ACS Nano **13**(7), 7985–7995 (2019).
15. X. Li, W. Zhang, W. Y. Wang, X. Wu, Y. Li, X. Tan, D. L. Matera, B. M. Baker, Y. M. Paulus, X. Fan, and X. Wang, "Optical coherence tomography and fluorescence microscopy dual-modality imaging for in vivo single-cell tracking with nanowire lasers," Biomed. Opt. Express **11**(7), 3659–3672 (2020).
16. A. Yazdanyar, P. Zhang, C. Dolf, Z. Smit-McBride, W. Cary, J.A. Nolta, R.J. Zawadzki, N., Marsh-Armstrong, and Park, "Effects of intravitreal injection of human CD34 + bone marrow stem cells in a murine model of diabetic retinopathy," Exp. Eye Res. **190**, 107865 (2020).
17. J. B. Grimm, A. K. Muthusamy, Y. Liang, T. A. Brown, W. C. Lemon, R. Patel, R. Lu, J. J. Macklin, P. J. Keller, N. Ji, and L. D. Lavis, "A general method to fine-tune fluorophores for live-cell and in vivo imaging," Nat. Methods **14**(10), 987–994 (2017).
18. E. B. Miller, P. Zhang, K. Ching, E. N. Pugh Jr, and M. E. Burns, "In vivo imaging reveals transient microglia recruitment and functional recovery of photoreceptor signaling after injury," Proc. Natl. Acad. Sci. **116**(33), 16603–16612 (2019).
19. A. Nwaneshiudu, C. Kuschal, F. H. Sakamoto, R. R. Anderson, K. Schwarzenberger, and R. C. Young, "Introduction to confocal microscopy," J. Invest. Dermatol. **132**(12), 1–5 (2012).
20. N. G. Horton, K. Wang, D. Kobat, C. G. Clark, F. W. Wise, C. B. Schaffer, and C. Xu, "In vivo three-photon microscopy of subcortical structures within an intact mouse brain," Nat. Photonics **7**(3), 205–209 (2013).

Biomedical Optics EXPRESS

21. X. Shu, L. J. Beckmann, and H. F. Zhang, "Visible-light optical coherence tomography: a review," J. Biomed. Opt **22**(12), 1 (2017).
22. M. Ang, R. M. Werkmeister, J. Chua, D. Schmidl, V. A. Dos Santos, G. Garhöfer, J. S. Mehta, and L. Schmetterer, "Anterior segment optical coherence tomography," Prog. Retin. Eye Res. **66**, 132–156 (2018).
23. V. P. Nguyen, Y. Li, W. Qian, B. Liu, C. Tian, W. Zhang, Z. Huang, A. Ponduri, M. Tarnowski, X. Wang, and Y. M. Paulus, "Contrast agent enhanced multimodal photoacoustic microscopy and optical coherence tomography for imaging of rabbit choroidal and retinal vessels in vivo," Sci. Rep. **9**(1), 1–17 (2019).
24. V. P. Nguyen, W. Qian, Y. Li, B. Liu, M. Aaberg, J. Henry, W. Zhang, X. Wang, and Y. M. Paulus, "Chain-like gold nanoparticle clusters for multimodal photoacoustic microscopy and optical coherence tomography enhanced molecular imaging," Nat. Commun. **12**(1), 34 (2021).
25. A. Kumar, I. Mondal, P. Roy, and R. Poddar, "TiO2 nanoparticles as exogenous contrast agent for 1 μm swept source optical coherence tomography: an in vitro study," Laser Phys. **28**(3), 035601 (2018).
26. D. Dhar, M. Mohan, and R. Poddar, "Assessment of Gd2O3 nanoparticles as exogenous imaging contrast agent for swept source optical coherence tomography," Laser Phys. **30**(1), 015601 (2020).
27. M. Humar, A. Dobravec, X. Zhao, and S. H. Yun, "Biomaterial microlasers implantable in the cornea, skin, and blood," Optica **4**(9), 1080–1085 (2017).
28. N. Martino, S. J. Kwok, A. C. Liapis, S. Forward, H. Jang, H. M. Kim, S. J. Wu, J. Wu, P. H. Dannenberg, S. J. Jang, and Y. H. Lee, "Wavelength-encoded laser particles for massively multiplexed cell tagging," Nat. Photonics **13**(10), 720–727 (2019).
29. A. H. Fikouras, M. Schubert, M. Karl, J. D. Kumar, S. J. Powis, A. Di Falco, and M. C. Gather, "Non-obstructive intracellular nanolasers," Nat. Commun. **9**(1), 4817 (2018).
30. X. Wu, Q. Chen, P. Xu, Y. C. Chen, B. Wu, R. M. Coleman, L. Tong, and X. Fan, "Nanowire lasers as intracellular probes," Nanoscale **10**(20), 9729–9735 (2018).
31. X. Li, Y. Qin, X. Tan, Y. C. Chen, Q. Chen, W. H. Weng, X. Wang, and X. Fan, "Ultrasound modulated droplet lasers," ACS Photonics **6**(2), 531–537 (2019).
32. D. N. Roxby, H. Rivy, C. Gong, X. Gong, Z. Yuan, G. E. Chang, and Y. C. Chen, "Microalgae living sensor for metal ion detection with nanocavity-enhanced photoelectrochemistry," Biosens. Bioelectron. **165**, 112420 (2020).
33. Z. Yuan, X. Cheng, Y. Zhou, X. Tan, X. Gong, H. Rivy, C. Gong, X. Fan, W. J. Wang, and Y. C. Chen, "Distinguishing small molecules in microcavity with molecular laser polarization," ACS Photonics **7**(8), 1908–1914 (2020).
34. M. Schubert, L. Woolfson, I. R. Barnard, A. M. Dorward, B. Casement, A. Morton, G. B. Robertson, P. L. Appleton, G. B. Miles, C. S. Tucker, and S. J. Pitt, "Monitoring contractility in cardiac tissue with cellular resolution using biointegrated microlasers," Nat. Photonics **14**(7), 452–458 (2020).
35. H. Shi, Z. Zhang, X. Wang, R. Li, W. Hou, W. Bi, and X. Zhang, "Inhibition of autophagy induces IL-1β release from ARPE-19 cells via ROS mediated NLRP3 inflammasome activation under high glucose stress," Biochem. Biophys. Res. Commun. **463**(4), 1071–1076 (2015).
36. H. H. Ai, I. Ichinose, S.A. Jones, D.K. Mills, Y.M. Lvov, and X. Qiao, "Biocompatibility of layer-by-layer self-assembled nanofilm on silicone rubber for neurons," J. Neurosci. Methods **128**(1-2), 1–8 (2003).
37. V. A. Sinani, D. S. Koktysh, B. G. Yun, R. L. Matts, T. C. Pappas, M. Motamedi, S. N. Thomas, and N. A. Kotov, "Collagen coating promotes biocompatibility of semiconductor nanoparticles in stratified LBL films," Nano Lett. **3**(9), 1177–1182 (2003).
38. A. Maslov and C. Ning, "Modal gain in a semiconductor nanowire laser with anisotropic bandstructure," IEEE J. Quantum Electron. **40**(10), 1389–1397 (2004).
39. X. Wu, Q. Chen, P. Xu, L. Tong, and X. Fan, "Refractive index sensing based on semiconductor nanowire lasers," Appl. Phys. Lett. **111**(3), 031112 (2017).